International Geology Review
Publication details, including instructions for authors and subscription information:
http://www.tandfonline.com/loi/tigr20

Hydration and dehydration in the lower margin of a cold mantle wedge: implications for crust-mantle interactions and petrogeneses of arc magmas

Yi Chen [a] , Kai Ye [a] , Yu-Wen Wu [b] , Shun Guo [a] , Bin Su [a] & Jing-Bo Liu [a]

[a] State Key Laboratory of Lithospheric Evolution, Institute of Geology and Geophysics, Chinese Academy of Sciences , P.O. Box 9825, Beijing , 100029 , China

[b] School of Information, Beijing Wuzi University , Beijing , 101149 , China

Published online: 26 Mar 2013.

To cite this article: Yi Chen , Kai Ye , Yu-Wen Wu , Shun Guo , Bin Su & Jing-Bo Liu (2013) Hydration and dehydration in the lower margin of a cold mantle wedge: implications for crust-mantle interactions and petrogeneses of arc magmas, International Geology Review, 55:12, 1506-1522, DOI: 10.1080/00206814.2013.781732

To link to this article: http://dx.doi.org/10.1080/00206814.2013.781732

International Geology Review, 2013
Vol. 55, No. 12, 1506–1522, http://dx.doi.org/10.1080/00206814.2013.781732

Taylor & Francis
Taylor & Francis Group

Hydration and dehydration in the lower margin of a cold mantle wedge: implications for crust–mantle interactions and petrogeneses of arc magmas

Yi Chen[a]*, Kai Ye[a], Yu-Wen Wu[b], Shun Guo[a], Bin Su[a] and Jing-Bo Liu[a]

[a]*State Key Laboratory of Lithospheric Evolution, Institute of Geology and Geophysics, Chinese Academy of Sciences, P.O. Box 9825, Beijing 100029, China;* [b]*School of Information, Beijing Wuzi University, Beijing 101149, China*

(*Accepted 27 February 2013*)

Garnet orthopyroxenites from Maowu (Dabieshan orogen, eastern China) were formed from a refractory harzburgite/dunite protolith. They preserve mineralogical and geochemical evidence of hydration/metasomatism and dehydration at the lower edge of a cold mantle wedge. Abundant polyphase inclusions in the cores of garnet porphyroblasts record the earliest metamorphism and metasomatism in garnet orthopyroxenites. They are mainly composed of pargasitic amphibole, gedrite, chlorite, talc, phlogopite, and Cl-apatite, with minor anhydrous minerals such as orthopyroxene, sapphirine, spinel, and rutile. Most of these phases have high X_{Mg}, NiO, and Ni/Mg values, implying that they probably inherited the chemistry of pre-existing olivine. Trace element analyses indicate that polyphase inclusions are enriched in large ion lithophile elements (LILE), light rare earth elements (LREE), and high field strength elements (HFSE), with spikes of Ba, Pb, U, and high U/Th. Based on the P–T conditions of formation for the polyphase inclusions (~1.4 GPa, 720–850°C), we suggest that the protolith likely underwent significant hydration/metasomatism by slab-derived fluid under shallow–wet–cold mantle wedge corner conditions beneath the forearc. When the hydrated rocks were subducted into a deep–cold mantle wedge zone and underwent high-pressure–ultrahigh-pressure (HP–UHP) metamorphism, amphibole, talc, and chlorite dehydrated and garnet, orthopyroxene, Ti-chondrodite, and Ti-clinohumite formed during prograde metamorphism. The majority of LILE (e.g. Ba, U, Pb, Sr, and Th) and LREE were released into the fluid formed by dehydration reactions, whereas HFSE (e.g. Ti, Nb, and Ta) remained in the cold mantle wedge lower margin. Such fluid resembling the trace element characteristics of arc magmas evidently migrates into the overlying, internal, hotter part of the mantle wedge, thus resulting in a high degree of partial melting and the formation of arc magmas.

Keywords: cold mantle wedge; hydration and dehydration; polyphase inclusions; crust–mantle interactions; arc magmas

Introduction

Mantle wedges play a key role in crust–mantle interactions and the formation of arc magmatism in subduction zones. Arc magmas are formed by the partial melting of the mantle wedge, which is metasomatized by fluids or melts released from the underlying subduction oceanic slab (Plank and Langmuir 1993; Elliot *et al.* 1997; Churikova *et al.* 2001; Manning 2004). The composition of arc volcanoes is often used to decipher the compositions of fluids or melts released from the subducting oceanic slab (Plank and Langmuir 1993; Elliot *et al*. 1997; Churikova *et al.* 2001). However, the formation of arc magmas requires that their mantle wedge source be sufficiently hot, where P–T conditions are above the wet mantle solidus (Sekine and Wyllie 1982; Matsukage and Kubo 2003; Manning 2004). The structures of the mantle wedges above subducting oceanic slabs have been well established based on observations on modern subduction zones, such as seismic wave velocity (Billen and Gurnis 2001; Nakajima and Hasegawa 2004), heat flow (e.g. Kincaid and Sacks 1997; Furukawa and Tatsumi 1999), radiogenic heat production (Brady *et al.* 2006; Faccenda *et al.* 2008), olivine fabrics (Kneller *et al.* 2005), arc and back-arc magmas (Martinez and Taylor 2002; Garrido *et al.* 2007), and mantle xenoliths (Maury *et al.* 1992; Arai 2007). It is widely accepted that corner flows induced by asthenospheric convection and slab subduction commonly exist in modern mantle wedges above the ongoing subduction of oceanic slabs (Martinez and Taylor 2002; Kelemen *et al.* 2003; Taylor and Martinez 2003; Curri and Hyndman 2006). The viscous coupling between the convecting asthenospheric mantle wedge and the subduction slab drives a sheet of depleted mantle rocks underlying a back-arc basin or magmatic arc to convect toward the shallow, cold, and wet corner of the mantle wedge. Viscous coupling further drives the cooled sheet of the mantle to convect downward to deeper mantle along a channel between the asthenospheric mantle and the subduction slab (Martinez and

*Corresponding author. Email: chenyi@mail.iggcas.ac.cn

Taylor 2002; Kelemen *et al.* 2003; Curri and Hyndman 2006).

This mantle wedge layer just above the subduction slab remains cold and is generally under the wet solidus (hereafter referred to as the cold mantle wedge) during downward convection to the deep mantle and is therefore not the source region of arc magmas (e.g. Kelemen *et al.* 2003; Scambelluri *et al.* 2006; Ye *et al.* 2009). The fluids released from the underlying subduction slab will penetrate and are expected to react with the lower margin of this cold mantle wedge (a relatively thin zone along the slab–mantle interface); thus, the composition of the slab fluids is expected to change before they reach the overlying, internal, hotter part of the mantle wedge (Manning 2004). The shallow part of the cold mantle wedge beneath the forearc most likely experiences hydration by the aqueous fluid released from the underlying subduction slab (Schmidt and Poli 1998; Scambelluri *et al.* 2004, 2006). At sub-arc depth, however, the temperature at the tops of the subducted oceanic crusts is as high as 650–1000°C (e.g. Kelemen *et al.* 2003; Syracuse *et al.* 2010; van Keken *et al.* 2011). Accordingly, in this region, the deep part of the cold mantle wedge lower margin is relatively dry because most hydrous mantle minerals (e.g. antigorite, amphibole, and talc) are likely dehydrated at such P–T conditions (Schmidt and Poli 1998), although it is also expected to react with the slab-derived fluid/melt. Dehydration of hydrous phases such as antigorite and amphibole releases large ion lithophile element (LILE)-, Li-, and B-rich aqueous fluids, which are able to carry several components of arc magmas (Scambelluri *et al.* 2004, 2006). Therefore, the lower margin of the cold mantle wedge along the slab–mantle interface is the crucial region where crust–mantle interactions occur, and observations of the detailed reactions are crucial to understand the petrogeneses of arc magmas. However, the mantle wedge, especially the lower marginal zone of the cold mantle wedge, remains one of the least known domains in the subduction factory, due to the lack of suitable rock samples that can be exhumed to the Earth's surface in modern oceanic subduction zones. Because the subducted oceanic crust at sub-arc depth is much denser than the surrounding mantle (Chen *et al.* 2013b), the down-going cold mantle wedge is commonly recycled together with the subducting oceanic crust into the deeper mantle and is thus difficult to exhume back to the Earth's surface (Zhao *et al.* 2007; Zhao 2008). Therefore, although numerous studies have focused on corner flow and fluid–rock interactions in subduction zones, only a few are based on direct observations of suitable rock samples from the cold mantle wedge lower margin (Scambelluri *et al.* 2006; Ye *et al.* 2009).

In continental subduction–collision zones, the deeply subducted felsic continental crust is commonly exhumed back to the Earth's surface due to its lower density than the surrounding mantle (Ernst *et al.* 1997; Ernst 2001, 2005, 2006; Lapen *et al.* 2007). On the way back, the exhumed continental crust often scrapes pieces of metasomatized peridotite from the overlying cold mantle wedge to the Earth's surface. These fragments occur as lenses or blocks in ultrahigh-pressure (UHP) terranes composed of deeply subducted continental crust, such as the Dabieshan–Sulu UHP terrane in eastern China and the Caledonian and Variscan UHP terranes in Europe (e.g. Brueckner and Medaris 2000; Malaspina *et al.* 2006; Scambelluri *et al.* 2006; Scambelluri *et al.* 2008; Malaspina *et al.* 2009; Ye *et al.* 2009). These mantle wedge rocks provide a unique opportunity to directly observe the metasomatic reactions of the mantle wedge lower margin along the slab–mantle interface.

Detailed petrological and geochemical studies indicate that the Maowu garnet orthopyroxenites from the Dabieshan UHP terrane in eastern China were formed by metasomatic interactions between precursor mantle wedge refractory harzburgite or dunite and slab-derived fluid/melt (Malaspina *et al.* 2006, 2009; Chen *et al.* 2013a). Polyphase solid inclusions of orthopyroxene, pargasitic amphibole, gedrite, chlorite, talc, phlogopite, sapphirine, corundum, rutile, and apatite are preserved in the cores of garnet porphyroblasts in the garnet orthopyroxenites. Malaspina *et al.* (2006, 2009) proposed that these polyphase inclusions were formed by the precipitation of an aqueous fluid trapped by the UHP garnet, and that this aqueous fluid is a residual fluid following peridotite–hydrous melt reactions during UHP metamorphism. A recent work (Chen *et al.* 2013a) proposes that the Maowu UHP garnet orthopyroxenites experienced large-scale corner-flow convection in the mantle wedge, predating UHP metamorphism. These rocks are therefore good samples to investigate the fate and the interaction of crustally derived subduction fluid with mantle wedge peridotites.

In this article, we investigated garnet orthopyroxenites in the Maowu mafic–ultramafic complex body from the Dabieshan UHP terrane in eastern China. The metamorphic evolution of the Maowu garnet orthopyroxenites was established in our recent study (Chen *et al.* 2013a). This article will focus on the microtextural and compositional analyses of polyphase inclusions in porphyroblastic garnets. Our new data indicate that the polyphase inclusions were the earliest metasomatic products formed by interactions between the depleted mantle harzburgite or dunite protolith and the slab-derived fluid, corresponding to a process of continuous hydration in the shallow mantle wedge corner. These new data enable us to discuss the roles played by the cold mantle wedge lower margin in the processes of crust–mantle interaction and arc magmatism in subduction zones.

Geological background and petrography

The Dabieshan UHP metamorphic terrane is located in the southwestern part of the Dabieshan–Sulu Orogen in eastern China (Figure 1A). It was formed by subduction/collision

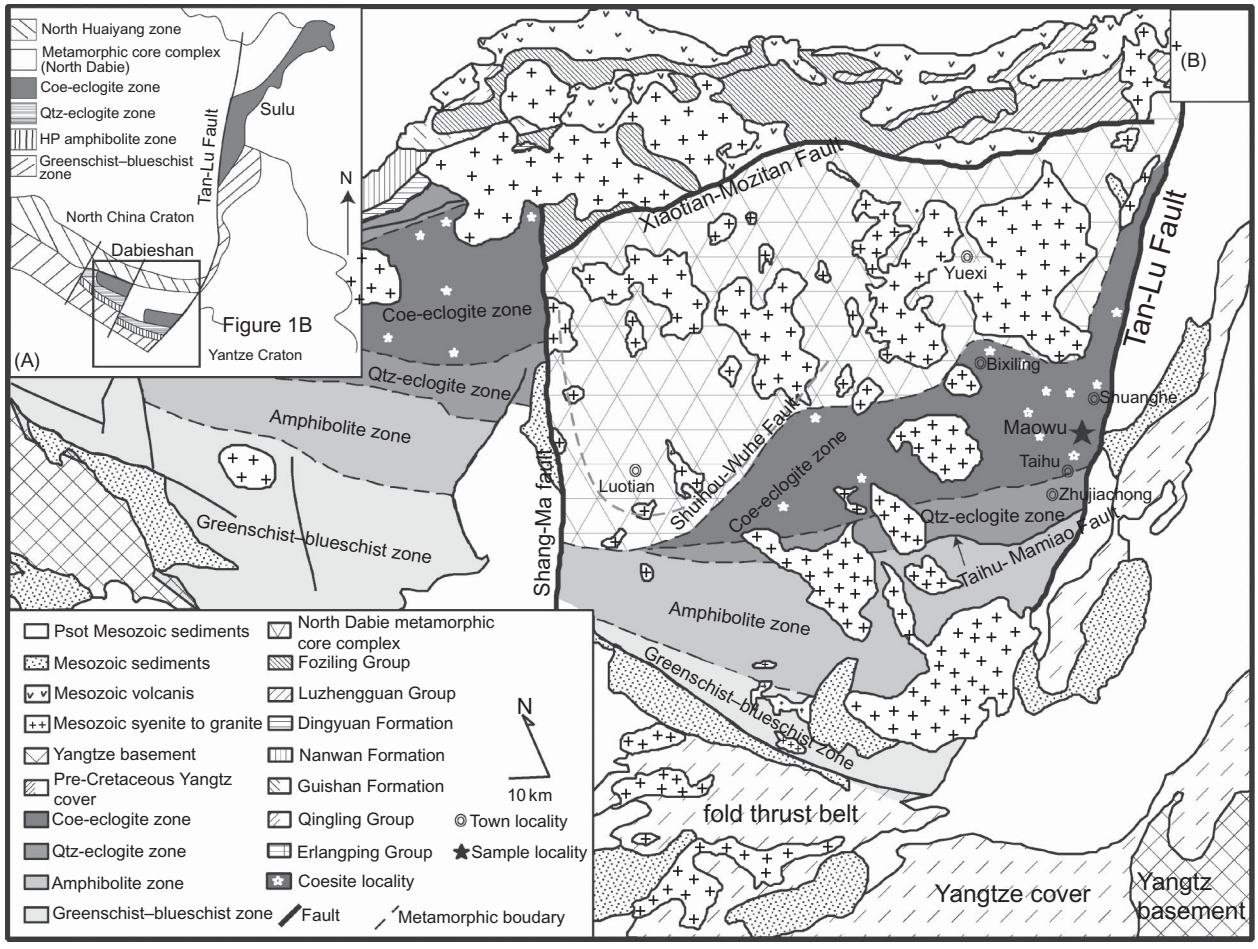

Figure 1. (A) Simplified index map of the Dabieshan Orogen in eastern China. (B) Geological sketch map of the Dabieshan Orogen in eastern China showing the locality of the Maowu mafic–ultramafic body.

of the Yangtze Craton beneath the Sino-Korean Craton in the Triassic (Li *et al.* 2000; Zheng *et al.* 2006). The Maowu mafic–ultramafic complex is a large E–W-trending lenticular body in paragneisses in the Dabieshan UHP metamorphic terrane (Figure 1B). This body is dominated by garnet orthopyroxenite and garnet-free orthopyroxenite with minor garnet clinopyroxenite, garnet websterite, harzburgite, and dunite. Relict olivine (Ol1) and minor orthopyroxene (Opx1) are preserved in the core of the matrix orthopyroxene (Opx2) in the garnet orthopyroxenite. The olivine (Ol1) and orthopyroxene (Opx1) have a similar composition to those in harzburgite/dunite, indicating that the protolith of garnet orthopyroxenite is a refractory harzburgite or dunite (Malaspina *et al.* 2006, 2009; Chen *et al.* 2013a). Polyphase solid inclusions were observed in the cores of garnet porphyroblasts (Malaspina *et al.* 2006, 2009; Chen *et al.* 2013a). Inductively coupled plasma mass spectrometry (ICP-MS) analysis shows that the trace element characteristics of the polyphase inclusions include high light rare earth element (LREE) contents and a pronounced enrichment in LILE, with spikes of Cs, Ba, and Pb (Malaspina *et al.* 2006, 2009). Based on these geochemical data, Malaspina *et al.* (2006) interpreted these inclusions as remnants of an aqueous fluid trapped by the UHP garnet.

Garnet orthopyroxenites rarely preserve textural and mineralogical evidence of six stages of metamorphism (Chen *et al.* 2013a): M_1 – high-T/low-P metamorphism (~1.4 GPa, ~850°C); M_2 – low-T/low-P metamorphism (~1.4 GPa, ~750°C); M_3 – low-T/high-P metamorphism (2.1–2.5 GPa, 740–760°C); M_4 – UHP metamorphism (5.3–6.3 GPa, ~800°C); M_5 – early retrogression (<3 GPa, >750°C); and M_6 – late retrogression (<2.3 GPa, <670°C). M_1–M_2 are interpreted as being related to corner flow in the mantle wedge above the subduction slab; M_2–M_4 are related to recycling of the rocks deep into upper mantle by downward flow; and M_4–M_6 are related to the uplift process by the exhumation of continental country rocks (Chen *et al.* 2013a).

Detailed petrography is described by Chen *et al.* (2013a). Here, the mineral assemblages and textures of the garnet orthopyroxenites from M_1 to M_4 are briefly summarized. The garnet orthopyroxenite samples studied are predominantly composed, in equilibrium, of medium-grained

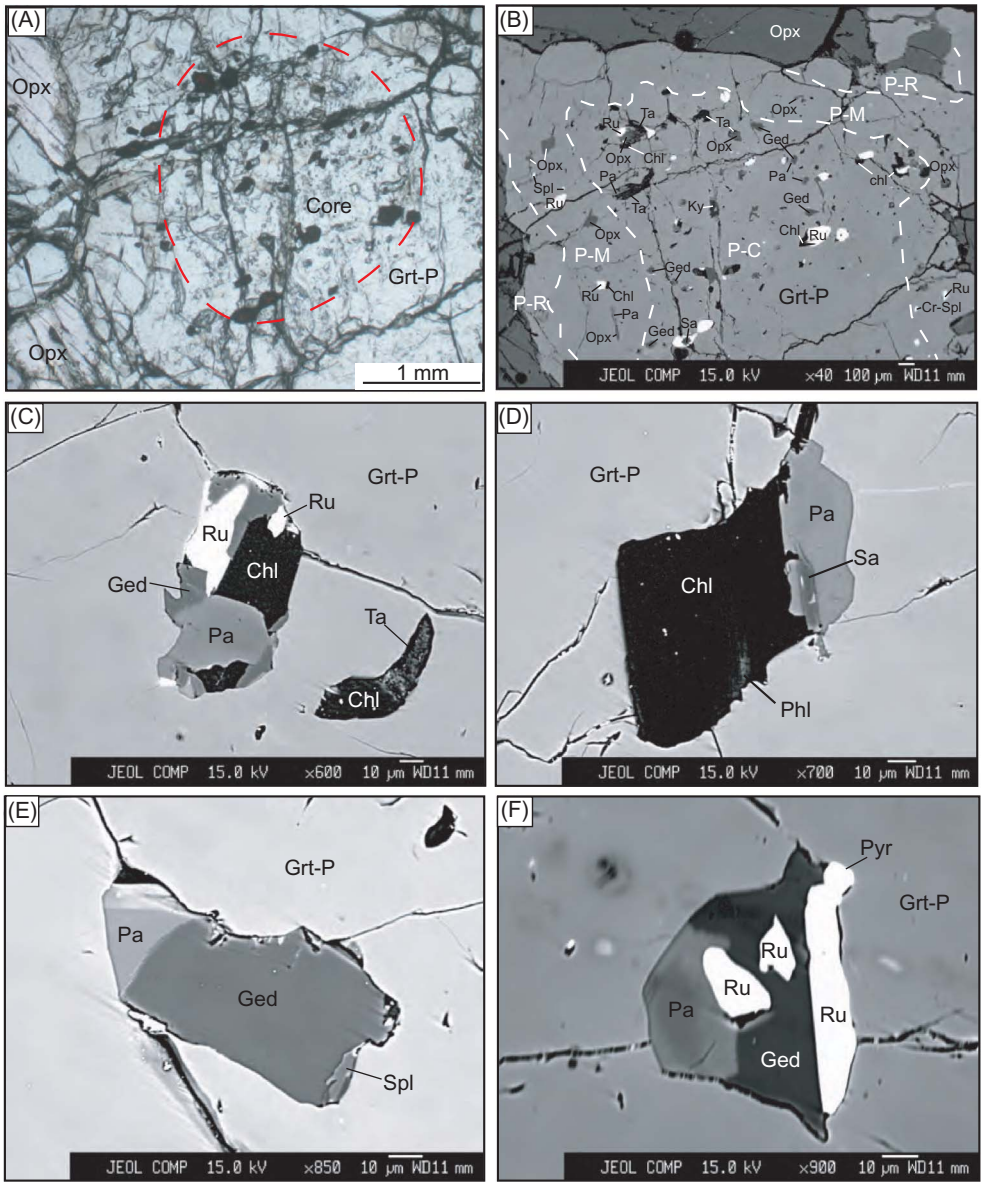

Figure 2. Photomicrograph (A) and back-scattered electron images (B–F) showing textures of the porphyroblastic garnet and inclusions inside. (A) Coarse-grained garnet porphyroblast occurs in garnet-rich orthopyroxenite. The core of garnet porphyroblast is dirty and contains inclusions. (B) Abundant polyphase inclusions are restricted to the core of garnet porphyroblast. Note that rutile is a common phase in these inclusions. (C) Polyphase inclusions of pargasitic amphibole, gedrite, chlorite, talc, and rutile. (D) Polyphase inclusions of sapphirine, pargasitic amphibole, chlorite, and phlogopite. (E) Polyphase inclusions of pargasitic amphibole, gedrite, and spinel. (F) Polyphase inclusions of pargasitic amphibole, gedrite, rutile, and pyrite. Grt, garnet; Opx, orthopyroxene; Pa, pargasitic amphibole; Ged, gedrite; Chl, chlorite; Ta, talc; Phl, phlogopite; Ky, kyanite; Sa, sapphirine; Spl, spinel; Ru, rutile; Pyr, pyrite.

(up to 2 mm) peak (M_4) UHP minerals of garnet and orthopyroxene with minor clinopyroxene, Ti-clinohumite, and Ti-chondrodite in the matrix; they constitute more than 95% of the rock volume, and the late overprint is very weak. Only minor rims of garnet and orthopyroxene are replaced by kelyphite of amphibole, spinel, chlorite, talc, and phlogopite. Rare porphyroblastic garnet (up to 1 cm) is preserved in the matrix peak UHP assemblages (Figure 2A).

Abundant polyphase inclusions within the core of porphyroblastic garnet (Figures 2A and 2B) are currently composed of hydrous phases (>70 vol.%) including gedrite, pargasite, chlorite, talc, apatite, and phlogopite. Rutile is a common phase in these inclusions. Anhydrous phases (<30%) in the inclusions contain rutile, sapphirine, garnet, corundum, spinel, orthopyroxene, and pyrite (Figures 2B–2F). The most common hydrous minerals are pargasite and gedrite. However, the infilling phases in the polyphase

inclusions are extremely heterogeneous, with mineral composition and volume proportions showing large variations (Figure 2B). Phlogopite was identified in rare cases. The centres of the polyphase inclusions are commonly characterized by a relatively drier assemblage (M_1) consisting of sapphirine + corundum + spinel + pargasite + orthopyroxene + garnet, whereas the rims of the polyphase inclusions usually contain a relatively wetter assemblage (M_2) of chlorite + talc + gedrite + pargasite + phlogopite + apatite + rutile + pyrite (see also Figure 2 in Chen *et al.* (2013a)). The mantles of porphyroblastic garnet (M_3) contain minor inclusions of chlorite, pargasite, orthopyroxene, spinel, and rutile. Gedrite and talc do not occur in these zones. The rims of the porphyroblastic garnet (M_4) are inclusion-free (Figure 2B).

Analytical techniques

Bulk-rock trace element concentrations were analysed on rock powders by ICP-MS using a Finnigan Mat Element Spectrometer at the Institute of Geology and Geophysics, Chinese Academy of Sciences, Beijing, China. Sample powders were digested in distilled HF + HNO_3 in 15 ml, high-pressure (HP) Savillex Teflon bombs at 120°C for 7 days, evaporated to near dryness and then diluted to 50 ml using super-pure HNO_3 for analysis. A blank solution was prepared, and the total procedural blank was used as an internal standard to correct for matrix effects and instrument drift. Precision for all trace elements is about 5%.

Major elements of rock-forming minerals were analysed by a JEOL 8100 microprobe analyser at the Institute of Geology and Geophysics, Chinese Academy of Sciences, Beijing, China. Analytical conditions were 15 kV accelerating voltage, 20 nA beam current, and 1.5 um beam size. The counting time for SrO in apatite and BaO in phlogopite was 30 s and that for other elements varied between 10 and 20 s. Phlogopite was measured at 5 nA with a defocused beam to prevent K devolatilization during the analyses. The precision of all analysed elements was better than 1.5%.

Mineral trace elements were analysed *in situ* on polished thin sections using a laser ablation inductively coupled plasma mass spectrometer (LA-ICP-MS) at the Institute of Geology and Geophysics, Chinese Academy of Sciences, Beijing, China. The analysis instrument included a Lambda Physik LPX 120I pulsed ArF excimer laser (193 nm) coupled to an Agilent 7500 ICP-MS. Helium was used as the carrier gas to enhance the transport efficiency of the ablated material. The out energy was about 80 mJ. Spot diameters varied between 44 and 120 μm according to grain dimensions. Counting times were approximately 20 and 40 s for background and analysis, respectively. ^{29}Si was used as the internal standard. The absolute content of SiO_2 in garnet was determined by the JEOL 8100 microprobe analyser described above. The SiO_2 of bulk solid inclusions was estimated by integrating the modal abundance information of the infilling phases and the host garnet. A glass standard NIST 610 (Pearce *et al.* 1997) was used as an external calibration standard. The external standard was analysed after every 10–15 analyses. The trace element data were calculated using the GLITTER 4.0 Online Interactive Data Reduction for LA-ICP-MS program, Macquarie University. Results obtained on the United States Geological Survey (USGS) rock standards indicate that the analysis accuracy is better than 5%.

The major elements of bulk solid inclusions were calculated by integrating the modal abundance of the infilling phases with the microprobe analyses. The modal abundance for each phase was obtained using the element mapping approach. To obtain the trace elements in the polyphase inclusions within the host garnet, we chose slightly larger spot sizes that just overlapped the bulk polyphase inclusions. The inclusions may occupy 30–65 vol.% of total volumes, whereas the host garnet comprises the remaining volumes. The trace elements of bulk solid inclusions were calculated based on the volume ratio of the inclusions/garnet and the composition of the host garnets. A similar approach was employed by Malaspina *et al.* (2006) and Gao *et al.* (2013).

Results

Whole-rock composition

Because garnet orthopyroxenites were formed from refractory harzburgite/dunite, we chose two samples of garnet orthopyroxenite (06MW11) and harzburgite (09MW38-1) for detailed analyses. The trace elements of whole-rock concentrations are listed in Table 1, and the chondrite (C1) normalized rare earth element (REE) and primitive mantle (PM) normalized trace element compositions are plotted in Figure 3.

Garnet orthopyroxenite shows a flat REE pattern (Figure 3A). The heavy rare earth element (HREE) concentrations are approximately 5 times the C1 values, due to the high proportion of garnet. The garnet orthopyroxenite is slightly enriched in Pb, Nb, and Ta, but the concentrations of some fluid-mobile LILE (e.g. Cs, Rb, Ba, and Sr) are relatively low (Figure 3B). The Nb and Ta concentrations in the garnet orthopyroxene are approximately 10 times the PM values. The REE concentrations and most trace elements are very low in the refractory harzburgite. Only Ba, U, Pb, Zr, and Hf show slight enrichment (Figure 3B), most likely due to late-stage overprinting by fluid derived from continental country rocks during exhumation (Chen *et al.* 2013a).

Host garnet chemistry

Representative major element compositions of the garnet porphyroblasts are listed in Table 2. The host garnet porphyroblasts commonly display three stages

Table 1. Trace element composition (ppm) of whole rocks and of representative garnet porphyroblasts.

Elements	Harzburgite	Grt opxenite	Grt P-C	Grt P-C	Grt P-M	Grt P-M	Grt P-R	Grt P-R
Li	1.68	1.04	n.a	n.a	n.a	n.a	n.a	n.a
Be	0.09	0.29	n.a	n.a	n.a	n.a	n.a	n.a
Sc	5.76	38.76	n.a	n.a	n.a	n.a	n.a	n.a
V	22.36	62.65	n.a	n.a	n.a	n.a	n.a	n.a
Cr	3210.56	4343.94	143.14	94.10	89.51	83.14	3639.14	2549.09
Co	119.29	83.28	n.a	n.a	n.a	n.a	n.a	n.a
Ni	2802.23	931.48	133	179	201	154	112	183
Cu	4.97	31.04	n.a	n.a	n.a	n.a	n.a	n.a
Zn	50.29	67.42	n.a	n.a	n.a	n.a	n.a	n.a
Ga	0.96	3.52	n.a	n.a	n.a	n.a	n.a	n.a
Rb	0.94	0.58	bdl	bdl	bdl	bdl	bdl	bdl
Sr	6.38	3.97	0.89	0.30	0.15	0.08	0.04	0.07
Y	0.42	6.90	33.33	29.80	39.67	41.91	17.13	18.19
Zr	9.84	10.62	1.48	4.76	1.24	1.43	2.09	2.23
Nb	0.22	3.53	bdl	bdl	bdl	bdl	bdl	bdl
Cs	0.02	0.02	n.a	n.a	n.a	n.a	n.a	n.a
Ba	20.10	2.24	0.49	0.53	0.05	0.11	0.03	0.05
La	0.21	1.13	0.02	0.03	0.01	0.02	0.04	0.04
Ce	0.64	2.10	0.03	0.04	0.02	0.03	0.05	0.06
Pr	0.04	0.34	0.03	0.02	0.04	0.05	0.02	0.03
Nd	0.18	1.96	0.39	0.23	0.42	0.54	0.25	0.23
Sm	0.05	0.57	1.15	1.22	0.83	0.92	0.43	0.50
Eu	0.02	0.19	0.76	0.84	0.84	0.80	0.36	0.33
Gd	0.08	0.80	3.66	3.01	5.51	4.79	2.13	2.35
Tb	0.01	0.17	0.85	0.78	1.14	1.15	0.41	0.46
Dy	0.09	1.20	6.16	5.21	7.62	7.53	2.93	3.32
Ho	0.02	0.26	1.40	1.17	1.48	1.53	0.67	0.73
Er	0.04	0.74	4.25	3.40	3.58	3.78	1.59	1.60
Tm	0.00	0.11	0.69	0.58	0.49	0.44	0.20	0.21
Yb	0.03	0.73	4.56	3.69	2.30	2.45	1.29	1.37
Lu	0.00	0.12	0.70	0.55	0.23	0.29	0.17	0.19
Hf	0.29	0.35	0.09	0.07	0.04	0.03	0.04	0.03
Ta	0.02	0.27	bdl	bdl	bdl	bdl	bdl	bdl
Pb	1.68	1.10	0.15	0.10	0.09	0.06	0.04	0.05
Th	0.07	0.01	0.03	0.02	0.03	0.04	0.03	0.02
U	0.05	0.04	bdl	bdl	bdl	bdl	bdl	bdl

Notes: n.a., not analysed; bdl, below detection limits; opxenite, orthoyroxenite; Grt, garnet; P, porphyroblast; C, core; M, mantle; R, rim.

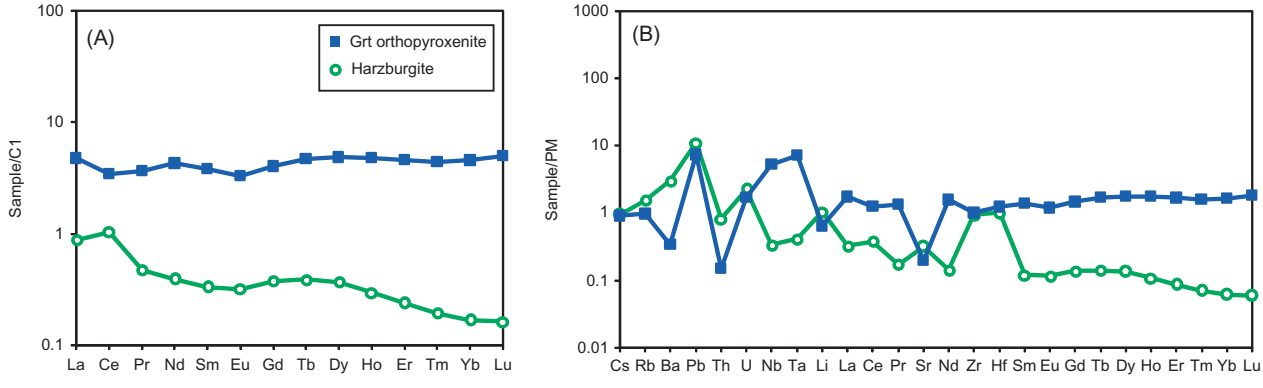

Figure 3. (A) Chondrite (C1) normalized bulk-rock REE patterns of garnet orthopyroxenite (06MW11) and harzburgite (09MW38-1). (B) Primitive mantle (PM) normalized trace element compositions of garnet orthopyroxenite (06MW11) and harzburgite (09MW38-1). Normalizing values are taken from Sun and McDonough (1989).

Table 2. Representative major element composition of infilling phases in polyphase inclusions and garnet porphyroblasts.

Mineral	Grt	Grt	Grt	Opx Incl. in Grt	Sa Incl. in Grt	Pa Incl. in Grt	Ged Incl. in Grt	Chl Incl. in Grt	Ta Incl. in Grt	Phl Incl. in Grt	Ap Incl. in Grt
Texture	P-C	P-M	P-R	P-C	P-C	P-C	P-C	P-C	P-C	P-C	P-C
SiO_2	42.20	41.51	41.56	57.78	11.60	44.93	45.07	32.99	61.40	38.73	0.07
TiO_2	0.08	0.00	0.05	0.00	0.01	0.37	0.07	0.03	0.00	1.09	0.00
Al_2O_3	23.68	23.78	22.67	0.97	67.17	16.96	20.11	20.00	0.58	17.40	0.00
Cr_2O_3	0.04	0.03	1.22	0.00	0.14	0.14	0.24	0.12	0.05	0.22	0.00
FeO	11.45	11.33	11.59	5.81	2.68	3.72	4.78	1.96	1.33	3.68	0.28
MnO	0.36	0.43	0.41	0.08	0.04	0.00	0.08	0.00	0.03	0.01	0.02
MgO	19.09	19.67	20.00	35.07	18.26	17.07	24.31	34.21	32.72	23.17	0.02
CaO	3.56	2.95	2.59	0.06	0.03	12.30	0.46	0.04	0.06	0.00	49.79
SrO	n.a.	n.a.	n.a.	n.a.	n.a.	n.a.	n.a.	n.a.	n.a.	n.a.	2.63
Na_2O	0.02	0.00	0.00	0.00	0.00	1.91	2.04	0.02	0.03	0.58	0.00
K_2O	0.00	0.01	0.00	0.01	0.00	0.17	0.01	0.00	0.02	8.13	0.00
NiO	0.02	0.00	0.00	0.14	0.05	0.17	0.07	0.07	0.11	0.13	0.00
BaO	n.a.	n.a.	n.a.	n.a.	n.a.	n.a.	n.a.	n.a.	n.a.	1.77	n.a.
P_2O_5	n.a.	n.a.	n.a.	n.a.	n.a.	n.a.	n.a.	n.a.	n.a.	n.a.	40.51
F	n.a.	n.a.	n.a.	n.a.	n.a.	0.00	0.00	0.00	0.00	0.00	0.00
Cl	n.a.	n.a.	n.a.	n.a.	n.a.	0.30	0.03	0.07	0.01	0.36	6.37
Total	100.51	99.71	100.08	99.92	99.97	98.03	97.26	89.52	96.34	95.27	99.69
O	12	12	12	6	20	23	23	14	11	11	13
Si	3.003	2.968	2.971	1.987	1.348	6.286	6.137	2.992	3.882	2.760	0.006
Ti	0.004	0.000	0.003	0.000	0.001	0.039	0.007	0.002	0.000	0.059	0.000
Al	1.986	2.004	1.910	0.039	9.207	2.796	3.227	2.138	0.044	1.461	0.002
Cr	0.002	0.001	0.069	0.000	0.013	0.015	0.026	0.008	0.003	0.012	0.000
Fe	0.682	0.677	0.693	0.167	0.261	0.435	0.544	0.149	0.070	0.219	0.021
Mn	0.022	0.026	0.025	0.002	0.003	0.000	0.009	0.000	0.001	0.001	0.002
Mg	2.025	2.096	2.132	1.798	3.163	3.560	4.935	4.626	3.084	2.461	0.003
Ca	0.271	0.226	0.198	0.002	0.004	1.844	0.067	0.004	0.004	0.000	4.766
Sr											0.136
Na	0.003	0.001	0.000	0.000	0.000	0.519	0.538	0.004	0.004	0.080	0.000
K	0.000	0.001	0.000	0.001	0.000	0.030	0.001	0.000	0.001	0.739	0.000
Ni	0.001	0.000	0.000	0.004	0.005	0.000	0.000	0.000	0.000	0.000	0.000
Ba										0.049	
P											3.064
F						0.000	0.000	0.000	0.000	0.000	0.000
Cl						0.070	0.008	0.011	0.001	0.043	0.995
X_{Mg}	0.748	0.773	0.775	0.915	0.924	0.891	0.901	0.969	0.978	0.918	

Note: n.a., not analysed; P-C, core of porphyroblastic garnet; P-M, mantle of porphyroblastic garnet; P-R, rim of porphyroblastic garnet; incl., inclusion; Grt, garnet; Opx, orthopyroxene; Sa, sapphirine; Pa, pargasitic amphibole; Ged, gedrite; Chl, chlorite; Ta, talc; Phl, phlogopite; Ap, apatite.

of growth zones (Chen *et al.* 2013a). The cores of the garnet porphyroblasts (M_2), which contain the polyphase inclusions, are homogeneous and have very low Cr_2O_3 (0.01–0.05 wt.%) and MgO (19.12–19.73 wt.%) contents and high CaO (2.91–3.76 wt.%) and FeO (11.70–12.82 wt.%) contents. The garnet porphyroblast mantles (M_3) contain higher MgO (19.75–20.81 wt.%) and lower CaO (2.33–2.84 wt.%) and FeO (11.15–11.62 wt.%) than the cores. The rims (M_4) have the highest Cr_2O_3 (1.16–1.54 wt.%), representing the compositions of the peak UHP garnets (Chen *et al.* 2013a).

Representative trace element compositions of the garnet porphyroblasts are listed in Table 1. Chondrite (C1)-normalized REE patterns of the garnet porphyroblasts are plotted in Figure 4. These three stages of garnets share LREE-depleted and HREE-enriched patterns, with absolute HREE concentrations up to 10–30 times the C1 values. The cores of the garnet porphyroblasts (M_2) are homogeneous in both major (Chen *et al.* 2013a) and trace elements. However, they contain relatively more HREE than the HP mantles and UHP rims (Figure 4). The mantles of the garnet porphyroblasts (M_3) show high middle rare earth elements [MREE; $(MREE > HREE)_{chondrite}$, Figure 4], which were likely inherited from the precursor phases (e.g. MREE-rich amphiboles) during high-pressure prograde metamorphism (Spandler *et al.* 2003; Xiao *et al.* 2013). The rims of the garnet porphyroblasts (M_4) have the lowest MREE and HREE concentrations. Meanwhile, they also show a MREE-rich pattern similar to that of the garnet porphyroblast mantles.

Chemistry of infilling phases in polyphase inclusions

Representative major element compositions of the infilling phases in the polyphase inclusions are listed in Table 2. The orthopyroxene grains have high X_{Mg} (0.90–0.93),

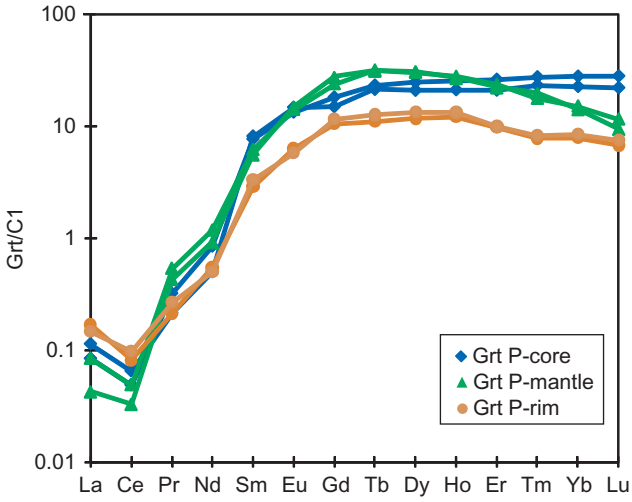

Figure 4. Chondrite normalized REE patterns for cores, mantles, and rims of porphyroblastic garnet. Normalizing values are taken from Sun and McDonough (1989).

Al (0.036–0.140 apfu), and NiO (0.12–0.22 wt.%) contents, and their Ni/Mg and Fe/Mn ratios can be compared with those of olivine. The sapphirine grains have high X_{Mg} (0.92–0.93) and detectable NiO (0.03–0.11 wt.%) and Cr_2O_3 (0.14–0.88 wt.%).

All hydrous phases in the polyphase inclusions (except apatite) have high X_{Mg} and NiO values, with detectable Cl (Table 2). However, their F contents are below the detectable limit. Consequently, their compositions are different from those F-bearing hydrous phases in kelyphite (M_6) after matrix garnet and orthopyroxene (Figure 5). The pargasitic amphibole has high X_{Mg} (0.89–0.90), NiO (0.11–0.20 wt.%), Na_2O (1.16–2.27 wt.%), and Cl (0.05–0.55 wt.%) and low K_2O (0.07–0.21 wt.%). The Na-gedrite contains high Al_2O_3 (18.04–22.31 wt.%) and Na_2O (1.91–2.68 wt.%), low CaO (0.31–0.50 wt.%) and TiO_2 (0.02–0.12 wt.%), and detectable Cl (0.01–0.04 wt.%). The chlorite contains high X_{Mg} (0.95–0.97), Al_2O_3 (19.88–22.52 wt.%), and FeO (1.64–2.01 wt.%) and detectable Cl (0.02–0.08 wt.%). The talc contains relatively high X_{Mg} (0.97–0.98), NiO (0.11–0.33 wt.%), and Al_2O_3 (0.58–1.07 wt.%) and detectable Cl (0.01–0.03 wt.%). The rare phlogopite crystals contain high X_{Mg} (0.92–0.93), BaO (1.42–1.77 wt.%), NiO (0.13–0.24 wt.%), and Cl (0.27–0.36 wt.%) (Figure 5). The tiny apatite crystals are extremely chlorine-rich (Cl: 4.82–6.37 wt.%) and contain considerable amounts of SrO (0.88–2.63 wt.%) with minor F (<0.51 wt.%) and FeO (0.08–0.28 wt.%).

Bulk composition of polyphase inclusions

We calculated the major element compositions in 30 polyphase inclusions based on the volume proportions and compositions of the infilling phases in the polyphase inclusions. Representative compositions of the bulk polyphase inclusions are listed in Table 3 and plotted in Figure 6. Figure 6 shows that the bulk major elements of these inclusions have large variations: SiO_2 = 33.27–53.39 wt.%, TiO_2 = 0.03–33.14 wt.%, Al_2O_3 = 8.43–29.46 wt.%, FeO = 2.15–4.64 wt.%, MgO = 17.48–29.87 wt.%, CaO = 0.20–4.99 wt.%, Na_2O = 0.05–2.29 wt.%, K_2O = 0.01–0.04 wt.%, and NiO = 0.07–0.17 wt.%. These large variations are caused by different proportions of infilling minerals from each polyphase inclusion. The large variation in TiO_2 content is attributed to different proportions of rutile in the inclusions. The low K_2O content may be caused by the very low proportion of phlogopite and relatively low K_2O content in amphibole. Although the polyphase inclusions have significantly different compositions, they systematically contain high X_{Mg} (0.89–0.98) and Ni/Mg (0.0011–0.0032) (Figure 6H). It is worth noting that SiO_2 and MgO contents show a positive correlation, which is different from the crystallization of fluids or melts (Figure 6A).

To obtain the trace element compositions of polyphase inclusions, we conducted laser ablation analyses of bulk inclusions. Laser spot sizes are larger than inclusions to cover the bulk inclusion, so the analytical results are a mixture of host garnet and polyphase inclusions. Garnet is an index mineral sink for HREE, but its LILE and LREE concentrations are generally low (e.g. Rubatto and Hermann 2003; Gao *et al.* 2013). Therefore, the HREE concentration of the mixtures (polyphase inclusions and host garnet) is mainly contributed by host garnet, whereas LILE and LREE concentrations mainly reflect the contribution of polyphase inclusions. Representative trace element composition of the mixtures is listed in Table 4. Figure 7 shows the PM normalized trace element composition of the mixture compared with an average pattern of inclusion-free domains in host garnet (restricted to the core of porphyroblastic garnet). Similar to the major element compositions, the trace element composition of the mixtures also exhibits significant variation, most likely due to either the different volume proportions of the infilling phases in different inclusions or the different volume proportions of inclusions affected by the laser with respect to host garnet. However, all of the mixtures show enrichment in LILE and LREE with respect to host garnet. The LILE abundances are approximately >10 times the PM values, with spikes of Ba, Pb, and U up to 10–100 times the PM values. The U/Th is relatively high (0.3–21). Some mixtures also exhibit enrichment of Nb and Ta due to the occurrence of rutile in the polyphase inclusions. The above features indicate that LILE, LREE, and high field strength element (HFSE) abundances of the mixtures mainly reside in polyphase inclusions.

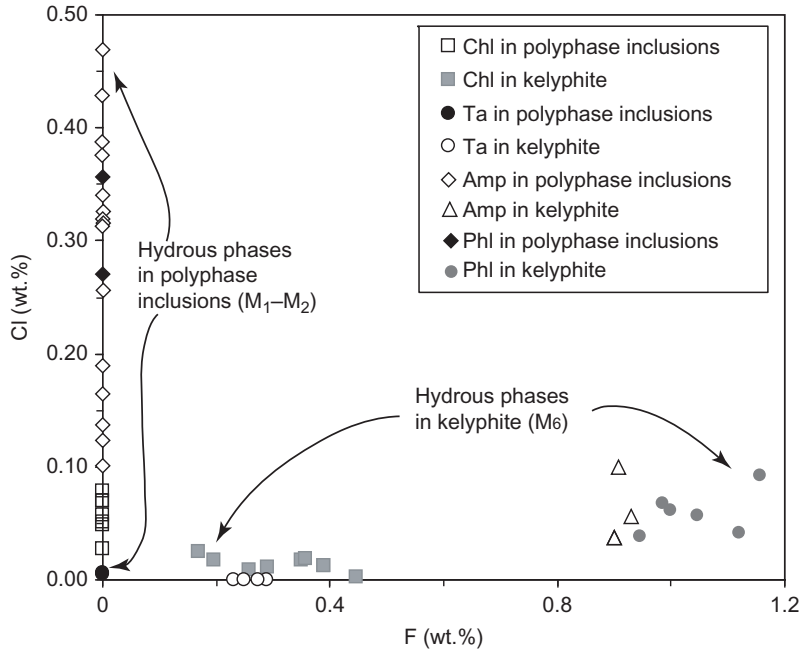

Figure 5. Variation in F wt.% and Cl wt.% in hydrous minerals from the Maowu garnet orthopyroxenite. Note that all of the hydrous minerals in the polyphase inclusions (M_1–M_2) are Cl-rich, and F was not detected in these minerals. The hydrous minerals in kelyphite (M_6) after the matrix garnet and orthopyroxene are F-rich.

Table 3. Calculated major element composition of representative polyphase inclusions.

Infilling phases	Chl + Ged + Pa + Ru	Chl + Pa + Sa + Spl	Chl + Ged + Pa + Ta + Opx	Ged + Pa + Spl + Ru	Ged + Pa + Ta + Ky + Ap	Chl + Ged + Pa + Rut + Spl	Ged + Pa + Ta + Opx	Ged + Pa + Ru + Spl + Phl
SiO_2	33.27	38.30	47.15	42.95	45.19	32.18	53.39	43.15
TiO_2	18.83	0.07	0.04	0.18	0.07	10.48	0.03	1.34
Al_2O_3	14.45	19.33	11.13	21.88	23.63	20.76	8.43	20.29
FeO	2.65	2.74	2.23	4.47	3.23	3.11	3.93	4.29
MgO	20.94	26.56	29.87	23.25	17.48	24.22	29.54	22.22
CaO	3.67	5.00	2.72	1.84	5.66	2.42	1.29	3.32
Na_2O	0.93	0.68	0.41	2.21	1.43	0.85	0.88	2.08
K_2O	0.03	0.03	0.03	0.02	0.04	0.02	0.02	0.04
NiO	0.09	0.13	0.17	0.06	0.12	0.09	0.16	0.08
Total	94.85	92.84	93.75	96.86	96.84	94.12	97.66	96.80

Note: Mineral abbreviations are the same as in Figure 2 and Table 2.

Discussion and conclusions

Origin of polyphase inclusions

The formation mechanism of polyphase inclusions in mantle rocks can be classified into two groups: (1) possible remnants of fluids or melts that have been entrapped by mantle rocks during or predating the peak HP/UHP metamorphism (e.g. Malaspina *et al.* 2006; Naemura *et al.* 2009) and (2) early fragment phases during the host mineral growth predating the subduction process (e.g. Okay 1994; Liou and Zhang 1998; Yang and Powell 2008; Chen *et al.* 2013a).

The origin of the polyphase inclusions in the Maowu garnet pyroxenites has been debated for approximately 20 years. Okay (1994), Liou and Zhang (1998), and Chen *et al.* (2013a) interpreted polyphase inclusions as relict early phases predating the Triassic subduction. Based on detailed mineralogical and petrological investigations, Chen *et al.* (2013a) suggest that polyphase inclusions record early two-stage metamorphism (M_1–M_2) prior to Triassic subduction, corresponding to an isobaric cooling process from ~850°C to ~750°C at ~1.4 GPa. However, Malaspina *et al.* (2006, 2009) proposed an alternative viewpoint. They assumed that these polyphase inclusions were

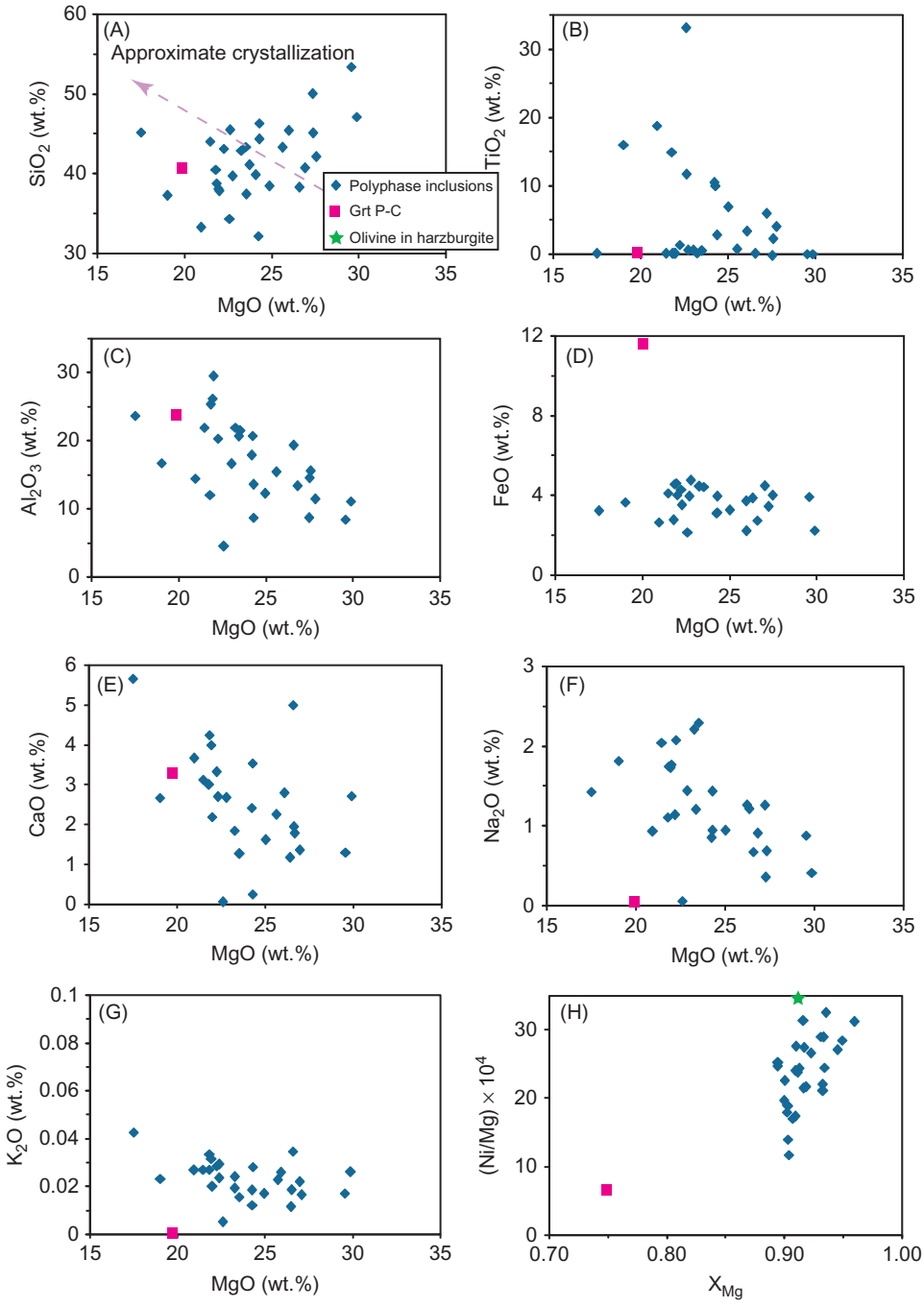

Figure 6. MgO (wt.%) *versus* major element oxides (wt.%) (A–G) and X_{Mg} *versus* Ni/Mg (H) for bulk polyphase inclusions. The major element compositions of bulk polyphase inclusions are calculated based on volume proportions and compositions of infilling phases. The average composition of host garnet in garnet orthopyroxenite and protolith olivine in harzburgite are also shown.

formed by the precipitation of an aqueous fluid trapped by the UHP garnet. Here, we provide the following microtextural and compositional evidence to corroborate the viewpoint of Chen *et al.* (2013a).

(1) Our petrological observations indicate that polyphase inclusions are restricted only in the cores of the zoned garnet porphyroblasts. If polyphase inclusions had been precipitated from UHP aqueous fluid (Malaspina *et al.* 2006, 2009), it is expected that they would have been trapped by any UHP minerals such as the microdiamond-bearing polyphase inclusions hosted by UHP garnet and pyroxene in garnet websterites from the Western Gneiss Region (Carswell and van

Table 4. Trace element composition (ppm) of representative mixtures (polyphase inclusion + garnet).

No.	A103	A107	A109	A114	A139	A152	A160	A162
K	287	429	218	194	388	210	147	1324
Rb	1.62	1.63	1.26	2.26	2.59	2.00	1.59	4.07
Sr	15.80	18.31	11.54	23.81	35.46	17.33	15.01	29.47
Y	21.25	20.52	20.42	19.54	15.90	15.51	15.83	18.66
Zr	22.23	2.13	2.21	2.42	1.74	18.55	3.47	4.15
Nb	94.88	0.28	0.25	1.19	0.12	79.22	0.31	9.85
Ba	90.70	120.72	73.28	69.93	200.80	91.70	62.55	120.79
La	0.25	0.22	0.26	0.72	0.48	0.40	0.46	0.62
Ce	0.40	0.34	0.35	0.64	1.08	0.46	0.58	0.60
Pr	0.11	0.08	0.09	0.21	0.11	0.16	0.13	0.19
Nd	0.68	0.51	0.59	1.22	0.65	0.93	0.78	1.09
Sm	0.93	0.69	0.80	1.74	0.90	1.20	1.04	1.55
Eu	0.35	0.28	0.31	0.55	0.16	0.40	0.35	0.49
Gd	2.16	1.83	1.99	3.02	0.89	2.35	2.04	2.73
Tb	0.48	0.44	0.45	0.50	0.18	0.43	0.39	0.47
Dy	3.58	3.43	3.49	3.08	1.28	2.78	2.66	2.96
Ho	0.86	0.82	0.83	0.75	0.31	0.67	0.64	0.72
Er	2.59	2.50	2.53	2.20	0.92	2.00	1.91	2.12
Tm	0.43	0.40	0.38	0.45	0.16	0.37	0.35	0.42
Yb	2.78	2.53	2.59	3.04	1.06	2.35	2.23	2.83
Lu	0.44	0.40	0.41	0.48	0.17	0.40	0.36	0.45
Hf	1.47	0.25	0.31	0.83	0.20	1.44	0.51	0.84
Ta	5.28	0.04	0.04	0.16	0.05	4.43	0.07	0.63
Pb	8.57	6.25	7.10	17.41	8.44	12.57	10.70	15.37
Th	0.08	0.08	0.11	0.11	0.26	0.12	0.11	0.10
U	1.75	0.03	0.03	0.09	0.14	1.48	0.04	0.24

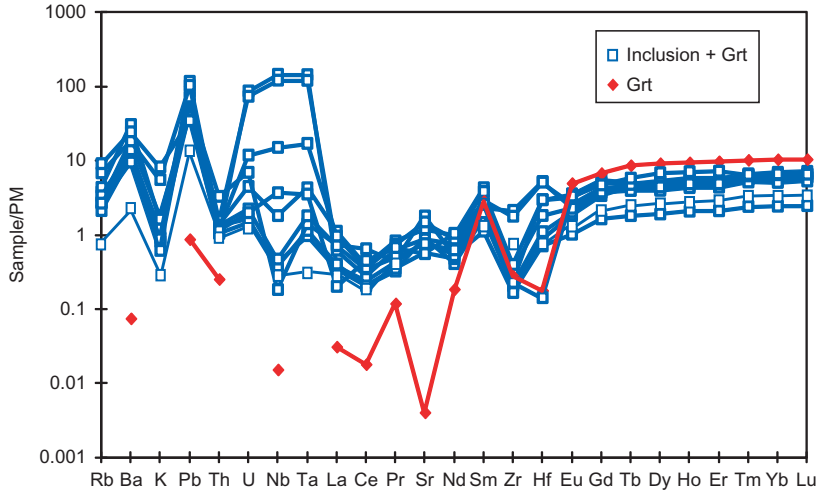

Figure 7. Primitive mantle (PM) normalized trace element compositions of the mixtures (polyphase inclusions and host garnet), compared with an average pattern of inclusion-free domains in the host garnet. Normalizing values are taken from Sun and McDonough (1989).

Roermund 2005). However, these inclusions never occur in the mantles and rims of zoned garnet porphyroblasts, and they are absent in the matrix garnet and orthopyroxene, which are also UHP minerals (M_4) (Chen *et al.* 2013a).

(2) As mentioned by Malaspina *et al.* (2006), the trapped-fluid hypothesis requires a constant volume proportion of the infilling phases and similar bulk composition of the polyphase inclusions; however, we checked more than 100 polyphase inclusions, and the volume proportion of the infilling phases in the inclusions is extremely heterogeneous. For example, some inclusions contain only a single amphibole grain; some are composed

of two grains of minerals, such as rutile + chlorite, rutile + sapphirine or pargasitic amphibole + gedrite, or chlorite + talc (Figures 2B and 2C); and others are composed of polyphases. The large variations in bulk major elements of inclusions (Figure 6) also support this point. Additionally, the positive correlation between bulk SiO_2 and MgO is in conflict with the scenario of crystallization from fluids or melts (Figure 6A). Therefore, these polyphase inclusions are not likely derived from a homogeneous trapped fluid.

(3) Considerable experimental data and natural observations imply that subduction zone UHP fluids/melts are mainly composed of SiO_2, Na_2O, Al_2O_3, and K_2O, with very limited FeO, MgO, and NiO, and very low X_{Mg} (e.g. Gao and Klemd 2001; Scambelluri and Philippot 2001; Manning 2004; Kessel *et al.* 2005a, 2005b; Guo *et al.* 2012; Gao *et al.* 2013). Polyphase inclusions are mainly composed (>90 vol.%) of Mg–Fe–Ca phases (Figure 2, Table 3), with total bulk MgO and FeO mostly higher than 25 wt.% (Figure 6). The 'mafic' bulk characteristics of polyphase inclusions are in conflict with the felsic characteristics of typical UHP fluid/melt derived from subducted crust.

(4) Malaspina *et al.* (2006) interpreted the bulk 'mafic' composition feature of polyphase inclusions as possibly having resulted from interaction between the assumed trapped fluid and host garnet during the retrograde decompression of rocks. However, different polyphase inclusions show distinct bulk inclusion compositions, and these compositions (including SiO_2, Al_2O_3, MgO, TiO_2, and NiO) differ from those of host garnet (Figure 6). Compared with host garnet, bulk polyphase inclusions contain higher MgO, Na_2O, K_2O, TiO_2, and NiO and lower Al_2O_3, FeO, and CaO (Figure 6). The compatible elements of Mg and Ni are likely difficult to modify during the decompression of host garnet because aqueous fluids cannot transport significant amounts of Mg and Ni. In this regard, polyphase inclusions would have MgO and NiO contents and a Ni/Mg ratio similar to those of host garnet. However, detailed compositional data indicate that polyphase inclusions contain relatively higher MgO, NiO, and Ni/Mg than host garnet (Table 2, Figure 6H). The high-Ni mafic minerals in polyphase inclusions could not be reaction products between host garnet and Mg–Ni-poor fluid. Moreover, retrograde reactions are expected to result in patchy garnet or retrograde zoning in host garnet in contact with polyphase inclusions (Perchuk *et al.* 2005). However, the cores of garnet porphyroblasts are generally homogeneous (Chen *et al.* 2013a). Our line (200–300 μm) traversing the garnet in contact with polyphase inclusions does not show any clear chemical zonation (for major or trace elements). Thus, we can rule out a later diffusional Ca–Fe–Mg exchange between host garnet and inclusion minerals.

(5) Both the mantles (M_3 and HP) and rims (M_4 and UHP) of garnet porphyroblasts exhibit a MREE-rich pattern (Figure 4) that is likely inherited from the precursor phases during high-pressure prograde metamorphism. Amphibole and titanite are typical MREE-rich phases in mafic–ultramafic rocks (Spandler *et al.* 2003; Xiao *et al.* 2013). In the Maowu garnet orthopyroxenites, amphibole is the major mineral in polyphase inclusions in the cores of garnet porphyroblasts (Figure 2), whereas titanite was not observed. On the other hand, only minor pargasitic amphibole and no gedrite occur in the mantles of the garnet porphyroblasts (Figure 2B), and amphibole never occurs in the rims. Therefore, the formation of garnet porphyroblast mantles and rims is most likely related to the breakdown of amphibole in the cores. Accordingly, the polyphase inclusions were formed earlier than the garnet porphyroblast mantles and rims formed during HP and UHP metamorphism.

Based on the above considerations, polyphase inclusions in the Maowu garnet orthopyroxenites were not likely formed by the precipitation of an aqueous fluid trapped by the host garnet. Petrological data show that polyphase inclusions represent the early two-stage metamorphism (M_1–M_2) (Chen *et al.* 2013a). Although the volume proportions of the infilling minerals are various in different polyphase inclusions, the same mineral in different polyphase inclusions has the same composition (Chen *et al.* 2013A). This characteristic indicates that the whole rock reached chemical equilibrium during M_1–M_2 metamorphism and that polyphase inclusions are relict fragments of the whole rock that escaped the impacts of later-stage metamorphism. The large variations in both major and trace element composition of polyphase inclusions are most likely attributable to the random capture of M_1–M_2 minerals by host pre-peak garnet.

Previous petrological data have indicated that the Maowu orthopyroxenites were derived from metasomatic interactions between precursor mantle refractory harzburgite or dunite and slab-derived siliceous fluid or hydrous melt (Malaspina *et al.* 2006, 2009; Chen *et al.* 2013A). This conclusion is supported by the texture, in which some relict olivine (Ol1) and minor Ni-poor orthopyroxene (Opx1) are preserved in the core of matrix Ni-rich orthopyroxene (Opx2) (Chen *et al.* 2013A). It is worth noting that this metasomatic texture is only preserved in garnet-poor orthopyroxenite, where garnet porphyroblasts and the polyphase inclusions do not occur.

This feature indicates that only protolith olivine (Ol1) in garnet-poor orthopyroxenite can survive during M_1–M_2 metamorphism. In garnet-rich orthopyroxenite where garnet porphyroblasts occur, the protolith Ol1 cannot be stable during M_1–M_2 metamorphism. Furthermore, the high X_{Mg} and Ni/Mg values of bulk polyphase inclusions may be consistent with those of Ol1 (Figure 6H). Fe–Mg minerals in polyphase inclusions, such as orthopyroxene, amphibole, sapphirine, chlorite, and talc have high NiO, high X_{Mg}, and low MnO contents (Table 2), indicating that they inherited the compositional features of the pre-existing olivine (Ol1). Therefore, we suggest that polyphase inclusions may be the earliest metasomatic products formed by interactions between protolith harzburgite/dunite and slab-derived fluid. Moreover, this study provides evidence that the formation mechanism of polyphase inclusions in mantle rocks should be carefully distinguished on the basis of their distribution textures, infilling and host minerals, and geochemical characteristics.

Hydration/metasomatism at the shallow–wet mantle wedge corner

Polyphase inclusions are characterized by the formation of abundant hydrous phases, and they record an isobaric cooling P–T path from M_1 (~1.4 GPa, ~850°C) to M_2 (1.3–1.5 GPa, 720–750°C) (Figure 9) (Chen *et al.* 2013a). Considering the refractory mantle harzburgite/dunite nature, we suggest that protolith peridotite likely undergoes significant hydration/metasomatism by slab-derived fluid at the shallow–wet mantle wedge corner beneath the forearc (Figure 9B).

Polyphase inclusions in M_1 and M_2 are enriched in fluid-mobile elements (Ba, Pb, and U) and display a high U/Th ratio (Figure 7) coupled with the crystallization of abundant hydrous phases (including amphibole, chlorite, and talc) during this process, suggesting that refractory peridotite was metasomatized by fluid released from the subducted crust and transformed to fertile rock. The formation of metasomatized phases, including orthopyroxene, sapphirine, corundum, Ba–Cl-rich amphibole, gedrite, chlorite, talc, rutile, Cl–Sr-rich apatite, and Fe–Ni-rich sulfides from the refractory harzburgite/dunite requires the additional components SiO_2, Al_2O_3, TiO_2, CaO, Na_2O, K_2O, P_2O_5, SrO, BaO, S, Cl, and H_2O, which are likely concentrated in the solute-rich fluid. The Cl-rich hydrous phases (apatite, amphibole, chlorite, and talc) in polyphase inclusions (Figure 5) reflect a Cl-rich metasomatized fluid because chlorine has high fluid/solid partition coefficients and only enters solid phases in significant amounts when the chlorinity of the fluid is very high (Zhu and Sverjensky 1991; Kullerud 1996; Markl and Bucher 1998; Kullerud *et al.* 2001; Xiao *et al.* 2005). Such Cl-rich subduction fluid has been observed in the shallow mantle wedge corner above the ongoing oceanic slab (Scambelluri *et al.* 2004).

Figure 8 shows the absolute concentrations of trace elements in polyphase inclusions calculated on the basis of inclusion/garnet volume proportions. The inclusion/garnet volume proportions were estimated using an element-mapping approach (Chen *et al.* 2013a). This approach is reasonable for the reduction of trace element data (especially LREE, LILE, and HFSE) of polyphase inclusions (Malaspina *et al.* 2006; Gao *et al.* 2013). Compared with protolith harzburgite, bulk polyphase inclusions exhibit significantly higher LILE, LREE, and HFSE (Figure 8). The increase in LILE (e.g. Ba, Pb, U, and Sr), LREE, and HFSE (Nb and Ta) during M_1–M_2 metamorphism likely reflects the fluid-mediated addition of crustal components to protolith peridotite. HFSE is commonly considered to be nominally fluid-immobile elements (Agapova *et al.* 1989; Tropper and Manning 2005). However, experimental studies conducted at $P \leq 2$ GPa

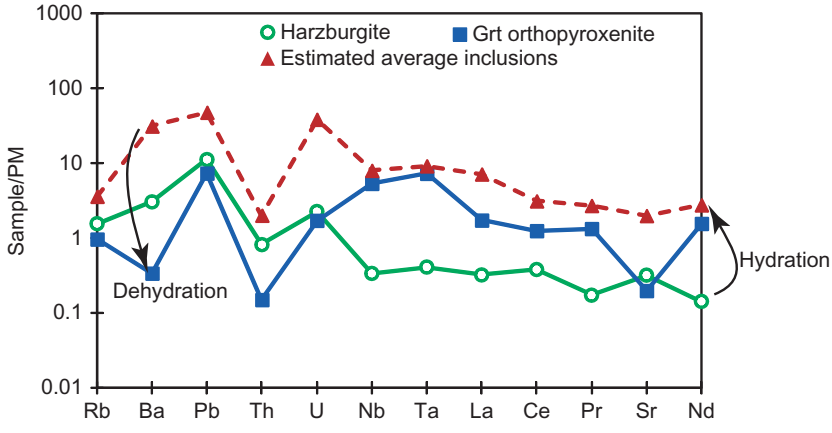

Figure 8. Primitive mantle (PM) normalized trace element patterns of average composition for polyphase inclusions calculated on the basis of inclusion/garnet volume proportions, compared with the composition of whole-rock garnet orthopyroxenite and protolith harzburgite.

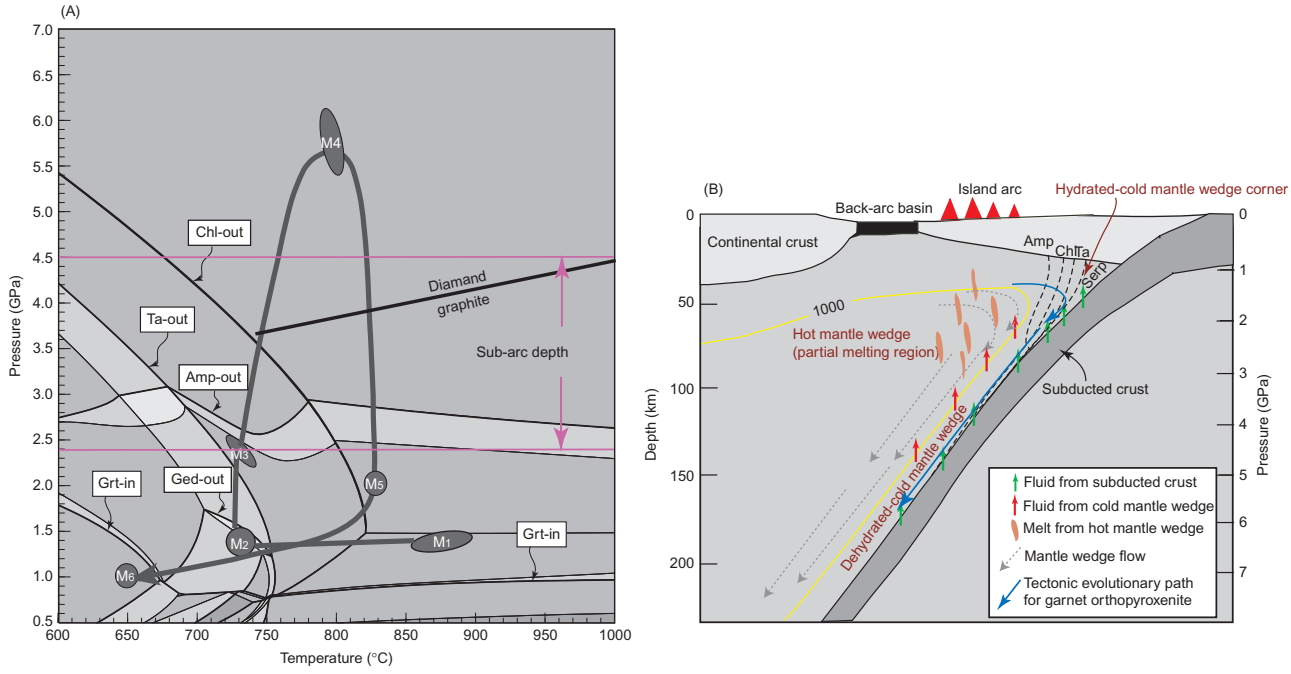

Figure 9. (A) P–T path (Chen *et al.* 2013a) for metamorphic evolution of Maowu garnet orthopyroxenite. Numbers refer to metamorphic stages according to Chen *et al.* (2013a). The region of sub-arc depth is after Manning (2004). Note that talc, amphibole, and chlorite are approximately dehydrated within sub-arc depth. (B) Schematic model of the structure of mantle wedge and tectonic evolution (M_1–M_4) of Maowu garnet orthopyroxenite. Green arrows indicate rise of fluid from subducted crust. Red arrows indicate rise of fluid from cold mantle wedge, which may be either fluid released by dehydration reactions of hydrous minerals in the cold mantle wedge lower margin, or residual aqueous fluid after reactions between cold mantle wedge peridotite and slab-derived fluid/melt. Yellow line represents the wet mantle solidus (~1000°C) (Schmidt and Poli 1998), and is the boundary between the cold and hot mantle wedges. Protolith harzburgite/dunite likely underwent significant hydration/metasomatism by crust-derived, LILE- and LREE-rich fluid at the shallow–wet–cold mantle wedge corner beneath the forearc. When the hydrated rock was subducted into a deep–cold mantle wedge zone under the arc, it became relatively dry and would release LILE (e.g. Ba, U, and Pb) and LREE into the fluid phase formed by dehydration reactions of the mantle hydrous minerals. Such LILE- and LREE-rich fluid evidently migrates into the overlying, internal, hotter part of the mantle wedge, thus resulting in a high degree of partial melting and the formation of arc magmas. Serp, serpentine; other mineral abbreviations are the same as in Figure 2.

(Antignano and Manning 2008; Manning *et al.* 2008) and natural observations of rutile in hydrothermal veins formed in subduction zones (e.g. Gao *et al.* 2001; John *et al.* 2008) demonstrate that subduction-zone fluids/melts rich in Na, Al, and Si can mobilize significant HFSE. The transport of HFSE in the metasomatized fluid during M_1–M_2 metamorphism may be attributed to its enrichment by SiO_2, Al_2O_3, and Na_2O.

The isobaric cooling P–T path corresponds to the corner-flow process above the subducting slab (Chen *et al.* 2013a). Thus, M_1 and M_2 minerals are most likely to represent continuously metasomatic phases during the corner-flow process. Such corner-flow motion is widely present in the mantle wedge above the ongoing subducting oceanic slab, bringing the rocks toward the subducting slab and into a fluid-rich P–T regime where fluids are released from the slab (Scambelluri and Philippot 2001; Manning 2004; Scambelluri *et al.* 2006; Arai and Ishimaru 2007; Ye *et al.* 2009). The scenario of hydration/metasomatism at the shallow–wet mantle wedge corner has also been reported in garnet peridotites in the Ulten zone of the eastern Italian Alps (Scambelluri *et al.* 2006; Scambelluri *et al.* 2010) and in those in the Sulu UHP terrane, eastern China (Ye *et al.* 2009).

The role of dehydration in the clod mantle wedge lower margin for the petrogeneses of arc magmas

The Maowu garnet orthopyroxenite remains cold (<850°C) in the deep upper mantle (Chen *et al.* 2013a). The stability of matrix UHP clinopyroxene, Ti-clinohumite, and Ti-chondrodite indicates that these rocks are under the wet mantle solidus at UHP conditions (Ulmer 2001; Matsukage and Kubo 2003) and, thus, can represent typical rocks in the lower margin of the cold mantle wedge just above the subducted slab. Such a cold mantle wedge underlying the sourced hot mantle of arc magmas and overlying the cold subduction slabs is commonly observed in modern oceanic subduction zones (Martinez and Taylor 2002; Kelemen *et al.* 2003; Curri and Hyndman 2006). Our petrological studies indicate that Maowu

garnet orthopyroxenite experienced strong metasomatism, hydration, and dehydration during the whole geodynamic processes. Observation of detailed metasomatic reactions may have very important implications for the petrogeneses of arc magmas.

When rocks were subducted into the deeper part of the cold mantle wedge zone (Figure 9B), the abundant hydrous minerals of amphibole, talc, and chlorite became unstable, and the minor Ti-chondrodite and Ti-clinohumite were the only stable hydrous minerals under UHP conditions (M_4). These observations indicate that dehydration reactions occurred and that a large amount of fluid must have been released from the lower margin of the cold mantle wedge. Petrological observations and pseudosection calculations (Chen *et al.* 2013a) indicate that along the deduced P–T path, talc, amphibole, and chlorite (the main hydrous minerals) will decompose at 2.3, 2.8, and 3.5 GPa, respectively (Figure 9A). These pressures are approximately echoed by the depth of the subduction slab just under the island arc (Manning 2004). The fluid released by dehydration reactions may also migrate into the overlying, hotter part of the mantle wedge (Figure 9B), thus resulting in a high degree of partial melting and the formation of arc magmas (Manning 2004).

Bulk rock analysis of M_1 and M_2 polyphase inclusions indicates that they are enriched in LREE and LILE and have significant spikes of Ba, U, and Pb (Figures 7 and 8). However, when rock is recycled into the deep–cold mantle wedge zone (M_4), only orthopyroxene, Ti-clinohumite, and Ti-chondrodite can accommodate minor LILE and LREE, and the rock is barely able to retain other incompatible elements (Jahn *et al.* 2003; Malaspina *et al.* 2006). This feature is also supported by the low incompatible element concentrations in garnet orthopyroxenite (Figure 8). Pre-peak polyphase inclusions in the cores of porphyroblastic garnet are generally rare (<1 vol.%) in whole garnet orthopyroxenite, and late-stage retrogression is very weak. Therefore, the whole-rock composition of garnet orthopyroxenite can approximately represent bulk-rock composition under peak UHP stage. From polyphase inclusions (M_1–M_2) to peak garnet orthopyroxenite (M_4), LILE (e.g. Ba, Pb, U, Sr, and Th) and LREE (e.g. La, Ce, and Pr) systematically decrease (Figure 8). However, HFSE (e.g. Nb and Ta) are not significantly changed and may be accommodated in peak Ti-clinohumite and Ti-chondrodite. This feature indicates that most LILE and LREE were released into the fluid formed by the dehydration reactions of hydrous minerals (Figure 9B), whereas HFSE likely remained in the cold mantle wedge lower margin. Such fluid resembles the trace element characteristics of arc magmas. Therefore, we suggest that hydration and dehydration at the lower edge of the cold mantle wedge must play very important roles in the formation of arc magmas. Further geochemical studies are required to reveal how this cold mantle wedge zone controls fluid–mantle interactions and related element mobility, partitioning, and fractionation.

Acknowledgements

This work was supported by the National Basic Research Programme of China (973 Programme 2009CB825001) and the National Science Foundation of China (Nos 40902023, 41090371, 40922150, and 41023009). Constructive comments from Professor J.H. Guo and Dr H.J. Xu improved the manuscript significantly. Drs Geoffrey and R. Timothy are thanked for polishing the language. Drs Q. Mao and Y.G. Ma are thanked for their help in electron microprobe analysis. This work benefited from discussions with Professors Z.M. Zhang and C.J. Wei.

References

Agapova, G.F., Modnikov, I.S., and Shmariovich, Y.M., 1989, Experimental study of the behavior of titanium in hot sulfide–carbonate solutions: International Geology Review, v. 31, p. 424–430.

Antignano, A., and Manning, C.E., 2008, Rutile solubility in H_2O, H_2O–SiO_2, and H_2O–$NaAlSi_3O_8$ fluids at 0.7–2.0 GPa and 700–1000°C: Implications for mobility of nominally insoluble elements: Chemical Geology, v. 255, p. 283–293.

Arai, S., and Ishimaru, S., 2007, Insights into petrological characteristics of the Lithosphere of mantle wedge beneath arcs through peridotite xenoliths: A review: Journal of Petrology, v. 49, p. 665–695.

Billen, M.I., and Gurnis, M., 2001, A low viscosity wedge in subduction zones: Earth and Planetary Science Letters, v. 193, p. 227–236.

Brady, R.J., Ducea, M.N., Kidder, S.B., and Saleeby, J.B., 2006, The distribution of radiogenic heat production as a function of depth in the Sierra Nevada Batholith, California: Lithos, v. 86, p. 229–244.

Brueckner, H.K., and Medaris, L.G., 2000, A general modal for the intrusion and evolution of 'mantle' garnet peridotite in high-pressure and ultrahigh-pressure metamorphic terranes: Journal of Metamorphic Geology, v. 18, p. 123–133.

Carswell, D.A., and Van Roermund, H.L.M., 2005, On multiphase mineral inclusions associated with microdiamond formation in mantle-derived peridotite lens at Bardane on Fjørtoft, west Norway: European Journal of Mineralogy, v. 17, p. 31–42.

Chen, Y., Ye, K., Guo, S., Wu, T.F., and Liu, J.B., 2013a, Multistage metamorphism of garnet orthopyroxenites from the Maowu mafic–ultramafic complex, Dabieshan UHP terrane, Eastern China: International Geology Review, doi:10.1080/00206814.2013.772694.

Chen, Y., Ye, K., Wu, T.F., and Guo, S., 2013b, Exhumation of oceanic eclogites: Thermodynamic constraints on pressure, temperature, bulk composition and density: Journal of Metamorphic Geology, doi:10.1111/jmg.12033.

Churikova, T., Dorendorf, F., and Wörner, G., 2001, Sources and fluids in the mantle wedge below Kamchatka, Evidence from across-arc geochemical variation: Journal of Petrology, v. 42, p. 1567–1593.

Currie, C.A., and Hyndman, R.D., 2006, The thermal structure of subduction zone back arcs: Journal of Geophysical Research, v. 111, p. 1–22.

Elliott, T., Plank, T., Zindler, A., White, W., and Bourdon, B., 1997, Element transport from slab to volcanic front at the Mariana arc: Journal of Geophysical Research, v. 102, p. 14991–15019.

Ernst, W.G., 2001, Ultra-high pressure metamorphism, and regurgitation of buoyant crustal slices: Implications for arcs and continental growth: Physics of the Earth and Planetary Interiors, v. 127, p. 253–275.

Ernst, W.G., 2005, Alpine and Pacific styles of Phanerozic mountain building: Subduction-zone petrogenesis of continental crust: Terra Nova, v. 17, p. 165–188.

Ernst, W.G., 2006, Preservation/exhumation of ultrahigh-pressure subduction complexes: Lithos, v. 92, p. 321–335.

Ernst, W.G., Maruyama, S., and Walis, S.R., 1997, Buoyancy-driven, rapid exhumation of ultrahigh-pressure metamorphosed continental crust: Proceedings of the National Academy of Sciences, v. 94, p. 9532–9537.

Faccenda, M., Gerya, T.V., and Chakraborty, S., 2008, Styles of post-subduction collisional orogen: Influence of convergence velocity, crustal rheology and radiogenic heat production: Lithos, v. 103, p. 257–287.

Furukawa, Y., and Tatsumi, Y., 1999, Melting of a subducting slab and production of high-Mg andesite magmas: Unusual magmatism in SW Japan at 13 approximately 15 Ma: Geophysical Research Letters, v. 26, p. 2271–2274.

Gao, J., and Klemd, R., 2001, Primary fluids entrapped at blueschist to eclogite transition: Evidence from the Tianshan meta-subduction complex in Northwest China: Contributions to Mineralogy and Petrology, v. 142, p. 1–14.

Gao, X.Y., Zheng, Y.F., Chen, Y.X., and Hu, Z., 2013, Trace element composition of continentally subducted slab-derived melt: Insight from multiphase solid inclusions in ultrahigh-pressure eclogite in the Dabie orogen: Journal of Metamorphic Geology, doi:10.1111/jmg.12029.

Garrido, C.J., Bodinier, J.L., Bhuime, B., Bosch, D., Chanefo, I., Bruguier, O., Hussain, S.S., Dawood, H., and Burg, J.P., 2007, Origin of the island arc Moho transition zone via melt–rock reaction and its implications for intracrustal differentiation of island arcs: Evidence from the Jijal complex (Kohistan complex, Northern Pakistan): Geology, v. 35, p. 683–686.

Guo, S., Ye, K., Chen, Y., Liu, J.B., Mao, Q., and Ma, Y.G., 2012, Fluid-rock interaction and element mobilization in UHP metabasalt: Constraints from an omphacite-epidote vein and host eclogites in the Dabie orogen: Lithos, v. 136, p. 145–167.

Jahn, B.M., Fan, Q.C., Yang, J.J., and Henin, O., 2003, Petrogenesis of the Maowu pyroxenite–eclogite body from the UHP metamorphic terrane of Dabieshan: Chemical and isotopic constraints: Lithos, v. 70, p. 243–267.

John, T., Klemd, R., Gao, J., and Garbe-Schönberg, C.-D., 2008, Trace-element mobilization in slabs due to non steady-state fluid–rock interaction: Constraints from an eclogitefacies transport vein in blueschist (Tianshan, China): Lithos, v. 103, p. 1–24.

Kelemen, P.B., Rilling, J.L., Parmentier, E.M., Mehl, L., and Hacker, B.R., 2003, Thermal structure due to solid-state flow in the Mantle wedge beneath arcs, *in* Eiler, J., ed., Inside the subduction factory: Geophysical monograph, Volume 138: Washington, D.C., AGU, p. 293–311.

Kessel, R., Schmidt, M.W., Ulmer, P., and Pettke, T., 2005a, Trace element signature of subduction-zone fluids, melts and supercritical liquids at 120–180 km depth: Nature, v. 437, p. 724–727.

Kessel, R., Ulmer, P., Pettke, T., Schmidt, M.W., and Thompson, A.B., 2005b, Experimental determination of phase relations and second critical endpoint in K-free eclogite-H_2O at 4–6 GPa and 700–1400°C: Earth and Planetary Science Letters, v. 237, p. 873–892.

Kincaid, C., and Sacks, I.S., 1997, Thermal and dynamical evolution of the upper mantle in subduction zones: Journal of Geophysical Research, v. 102, p. 12295–12315.

Kneller, E.A., van Keken, P.E., Karato, S., and Park, J., 2005, B-type olivine fabric in the mantle wedge: Insights from high-resolution non-Newtonian subduction zone models: Earth and Planetary Science Letters, v. 237, p. 781–797.

Kullerud, K., 1996, Chlorine-rich amphiboles: Interplay between amphibole composition and an evolving fluid: European Journal of Mineralogy, v. 8, p. 355–370.

Kullerud, K., Flaat, K., and Davidsen, B., 2001, High-pressure fluid–rock reactions involving Cl-bearing fluids in lower-crustal ductile shear zones of the Flakstadoy Basic Complex, Lofoten, Norway: Journal of Petrology, v. 42, p. 1349–1372.

Lapen, T.J., Johnson, C.M., Baumgartner, L.P., Dal Piaz, G.V., Skora, S., and Beard, B.L., 2007, Coupling of oceanic and continental crust during Eocene eclogite-facies metamorphism: Evidence from the Monte Rosa nappe, western Alps: Contribution to Mineralogy and Petrology, v. 153, p. 139–157.

Li, S.G., Jagoutz, E., Chen, Y.Z., and Li, Q.L., 2000, Sm–Nd and Rb–Sr isotopic chronology and cooling history of ultrahigh pressure metamorphic rocks and their country rocks at Shuanghe in the Dabie Mountains, Central China: Geochimica et Cosmochimica Acta, v. 64, p. 1077–1093.

Liou, J.G., and Zhang, R.Y., 1998, Petrogenesis of an ultrahigh-pressure garnet-bearing ultramafic body from Maowu, Dabie Mountains, Eastern-Central China: The Island Arc, v. 7, p. 115–134.

Malaspina, N., Hermann, J., and Scambelluri, M., 2009, Fluid/mineral interaction in UHP garnet peridotite: Lithos, v. 107, p. 38–52.

Malaspina, N., Hermann, J., Scambelluri, M., and Compagnoni, R., 2006, Polyphase inclusions in garner-orthopyroxenite (Dabie Shan, China) as monitors for metasomatism and fluid-related trace element transfer in subduction zone peridotite: Earth and Planetary Science Letters, v. 249, p. 173–187.

Manning, C.E., 2004, The chemistry of subduction-zone fluids: Earth and Planetary Science Letters, v. 223, p. 1–16.

Manning, C.E., Wilke, M., Schmidt, C., and Cauzid, J., 2008, Rutile solubility in albite–H_2O and $Na_2Si_3O_7$–H_2O at high temperatures and pressures by in-situ synchrotron radiation micro-XRF: Earth and Planetary Science Letters, v. 272, p. 730–737.

Markl, G., and Bucher, K., 1998, Metamorphic salt in granulites: Implications for the presence and composition of fluid in the lower crust: Nature, v. 391, p. 781–783.

Martinez, F., and Taylor, B., 2002, Mantle wedge control on back-arc crustal accreation: Nature, v. 416, p. 417–420.

Matsukage, K.N., and Kubo, K., 2003, Chromian spinel during melting experiments of dry peridotite (KLB-1) at 1.0–2.5 GPa: American Mineralogist, v. 88, p. 1271–1278.

Maury, R.G., Defant, M.J., and Joron, J.L., 1992, Metasomatism of the sub-arc mantle inferred from trace elements in Philippine xenoliths: Nature, v. 360, p. 661–663.

Naemura, K., Hirajima, T., and Svojtka, M., 2009, The pressure–temperature path and the origin of phlogopite in spinel-garnet peridotites from the Blansky Les Massif of the Moldanubian Zone, Czech Republic: Journal of Petrology, v. 50, p. 1795–1827.

Nakajima, J., and Hasegawa, A., 2004, Shear-wave polarization anisotropy and subduction-induced flow in the mantle wedge of Northeastern Japan: Earth and Planetary Science Letters, v. 225, p. 365–377.

Okay, A.I., 1994, Sapphirine and Ti-clinohumite in ultrahigh-pressure garnet-pyroxenite and eclogite from Dabie Shan,

China: Contributions to Mineralogy and Petrology, v. 116, p. 145–155.

Pearce, N.J.G., Perkins, W.T., Westgate, J.A., Gorton, M.P., Jackson, S.E., Neal, C.R., and Chenery, S.P., 1997, A compilation of new and published major and trace element data for NIST SRM 610 and NIST SRM 612 glass reference materials: Geostandards Newsletters, v. 21, p. 115–144.

Perchuk, A.L., Burchard, M., Maresch, W.V., and Schertl, H.P., 2005, Fluid-mediate modification of garnet interiors under ultrahigh-pressure conditions: Terra Nova, v. 17, p. 545–553.

Plank, T., and Langmuir, C.H., 1993, Tracing trace elements from sediment input to volcanic output at subduction zones: Nature, v. 362, p. 739–743.

Rubatto, D., and Hermann, J., 2003, Zircon formation during fluid circulation in eclogites (Monviso, Western Alps): Implications for Zr and Hf budget in subduction zones: Geochimica et Cosmochimica Acta, v. 67, p. 2173–2187.

Scambelluri, M., Hermann, J., Morten, L., and Rampone, E., 2006, Melt- versus fluid-induced metasomatism in spinel to garnet wedge peridotites (Ulten Zone, Eastern Italian Alps): Clues from trace element and Li abundances: Contributions to Mineralogy and Petrology, v. 151, p. 372–394.

Scambelluri, M., Muntener, O., Ottolini, L., Pettke, T., and Vannucci, R., 2004, The fate of B, Cl and Li in the subducted oceanic mantle and in the antigorite breakdown fluids: Earth and Planetary Science Letters, v. 222, p. 217–234.

Scambelluri, M., Pettke, T., and van Roermund, H.L.M., 2008, Majoritic garnets monitor deep subduction fluid flow and mantle dynamics: Geology, v. 36, p. 59–62.

Scambelluri, M., and Philippot, P., 2001, Deep fluids in subduction zones: Lithos, v. 55, p. 213–227.

Scambelluri, M., van Roermund, H.L.M., and Pettke, T., 2010, Mantle wedge peridotites: Fossil reservoirs of deep subduction zone processes influences from high and ultrahigh-pressure rocks from Bardane (Western Norway) and Ulten (Italian Alps): Lithos, v. 120, p. 186–201.

Schmidt, M.W., and Poli, S., 1998, Experimentally based water budgets for dehydrating slabs and consequences for arc magma generation: Earth and Planetary Science Letters, v. 163, p. 361–379.

Sekine, T., and Wyllie, P.J., 1982, The system granite–peridotite–H_2O at 30 kbar, with applications to hybridization between hydrous siliceous melts and peridotite: Contributions to Mineralogy and Petrology, v. 81, p. 190–202.

Spandler, C., Hermann, J., Arculus, R., and Mavrogenes, J., 2003, Redisteibution of trace elements during prograde metamorphism from lawsonite blueschist to eclogite facies: Implications for deep subduction-zone process: Contributions to Mineralogy and Petrology, v. 146, p. 205–222.

Sun, S.S., and McDonough, W.F. 1989, Chemical and isotopic systematics of oceanic basalts: Implications for mantle composition and processes, *in* Saunders, A.D., Norry, M.J., eds., Magmatism in the ocean basins: Geological Society Special Publications, 42, p. 313–345.

Syracuse, E.M., van Keken, P.E., and Abers, G.A., 2010, The global range of subduction zone thermal models: Physics of the Earth and Planetary Interiors, v. 51, p. 1761–1782.

Taylor, B., and Martinez, F., 2003, Back-arc basin basalt systematics: Earth and Planetary Science Letters, v. 210, p. 481–497.

Tropper, P., and Manning, C.E., 2005, Very low solubility of rutile in H_2O at high pressure and temperature, and its implications for Timobility in subduction zones: American Mineralogists, v. 90, p. 502–505.

Ulmer, P., 2001, Partial melting in the mantle wedge – the role of H_2O in the genesis of mantle-derived "arc-related" magmas: Physics in Earth Planetary Interiors, v. 127, p. 215–232.

van Keken, P.E., Hacker, B.R., Syracuse, E.M., and Abers, G.A., 2011, Subduction factory: 4. Depth-dependent flux of H_2O from subducting slabs worldwide: Journal of Geophysical Research, v. 116, B01401. doi:10.1029/2010JB007922.

Xiao, Y.L., Hoefs, J., and Kronz, A., 2005, Compositionally zoned Cl-rich amphiboles from North Dabie Shan, China: Monitor of high-pressure metamorphic fluid/rock interaction processes: Lithos, v. 81, p. 279–295.

Xiao, Y.Y., Niu, Y.L., Song, S.G., Davidson, J., and Liu, X.M., 2013, Element response to subduction-zone metamorphism: Constraints from the North Qilian Mountain, NW China: Lithos, v. 160–161, p. 55–67.

Yang, J.J., and Powell, R., 2008, Ultrahigh-pressure garnet peridotites from the devolatilization of sea-floor hydrated ultramafic rocks: Journal of Metamorphic Geology, v. 26, p. 695–716.

Ye, K., Song, Y.R., Chen, Y., Xu, H.J., Liu, J.B., and Sun, M., 2009, Multistage metamorphism of orogenic garnet-lherzolite from Zhimafang, Sulu UHP terrane, Eastern China: Implications for mantle wedge convection during progressive oceanic and continental subduction: Lithos, v. 109, p. 155–175.

Zhao, D.P., 2008, Multiscale seismic tomography and mantle dynamics: Gondwana Research, v. 15, p. 297–323.

Zhao, D.P., Maruyama, S., and Omori, S., 2007, Mantle dynamics of western Pacific to East Asia: New insight from seismic tomography and mineral physics: Gondwana Research, v. 11, p. 120–131.

Zheng, Y.F., Zhao, Z.F., Wu, Y.B., Zhang, S.B., Liu, X.M., and Wu, F.Y., 2006, Zircon U–Pb age, Hf and O isotope constraints on protolith origin of ultrahigh-pressure eclogite and gneiss in the Dabie orogen: Chemical Geology, v. 231, p. 135–158.

Zhu, C., and Sverjensky, D.A., 1991, Partitioning of F–Cl–OH between minerals and hydrothermal fluids: Geochimica et Cosmochimica Acta, v. 55, p. 1837–1858.